

Small-scale lateral variations in D'' attenuation and velocity structure

Jesse L. Fisher and Michael E. Wysession

Department of Earth and Planetary Science, Washington University, St. Louis, Missouri, USA

Karen M. Fischer

Department of Geological Sciences, Brown University, Providence, Rhode Island, USA

Received 27 August 2002; revised 16 December 2002; accepted 3 February 2003; published 26 April 2003.

[1] Combined ScS - S differential attenuation and travel-time studies, with data from temporary and permanent arrays, produce quality factor, $Q_{\mu}(D'')$, estimates for D'' beneath Central America. Similarities between S and ScS ray paths through the upper mantle reduce the upper mantle elastic and anelastic contributions to differential studies. Differential attenuation correlates with ScS attenuation but not S attenuation, indicating that the attenuation primarily stems from lower mantle interactions. We image a ~ 250 km wide high-attenuation low-velocity anomaly within a ~ 600 km wide low-attenuation high-velocity region at the core-mantle boundary (CMB). The observed inverse exponential relationship between attenuation and velocity is consistent with a 200 ± 50 km thermal anomaly, but does not preclude chemical, phase, or structural variations. Observation of a small-scale thermal anomaly within D'' may provide significant evidence in favor of one kind of plume formation at the CMB. **INDEX TERMS:** 5144 Physical Properties of Rocks: Wave attenuation; 7203 Seismology: Body wave propagation; 7207 Seismology: Core and mantle; 8121 Tectonophysics: Dynamics, convection currents and mantle plumes; 8124 Tectonophysics: Earth's interior—composition and state (8105). **Citation:** Fisher, J. L., M. E. Wysession, and K. M. Fischer, Small-scale lateral variations in D'' attenuation and velocity structure, *Geophys. Res. Lett.*, 30(8), 1435, doi:10.1029/2002GL016179, 2003.

1. Introduction

[2] The past 30 years of seismological research have revealed striking variations in thickness, P - and S -wave velocities, anisotropy, and velocity gradients within D'' on many length-scales [Garnero, 2000]. Nevertheless, many key questions remain unanswered regarding the properties of D'' . Are the observed variations within D'' thermally or chemically derived? How does D'' and the rest of the mantle interact? What effects do subducted slabs have on D'' ? Do some plumes originate within D'' ? This paper presents a method and case study that aids the identification and characterization of thermal contributions to D'' anomalies, and therefore provide improved investigations into these fundamental questions.

[3] This study analyzes the elastic (i.e. velocity) and anelastic (i.e. attenuation) properties of the lower mantle through a combined differential ScS - S travel-time and attenuation technique. The advantage of differential studies stems from the similarity between the S and ScS ray paths

through the crust and upper mantle and the removal of effects from uncertainties in source location and rupture processes. There are several benefits to examining attenuation in conjunction with travel-time. 1) The dispersive effects of attenuation alter travel-time measurements [Kuo *et al.*, 1987; Karato, 1993]. 2) Attenuation in the upper mantle varies exponentially with temperature (relative to the homologous temperature), while velocity is inversely proportional to temperature [Karato and Spetzler, 1990]. We assume these relationships are true for the lower mantle as well. The exponential nature of attenuation makes combined studies more sensitive to thermal anomalies than pure travel-time studies. 3) The respective linear and exponential relationships of elastic and anelastic properties provide a basis to distinguish between thermal and chemical anomalies. The observation of an inverse exponential relationship between attenuation and velocity may indicate variations of temperature [Romanowicz, 1995].

[4] The indication of a thermal anomaly through the use of our technique may provide evidence for plume formation, mantle- D'' interactions, or phase change. Variations in temperature relative to homologous temperature, measured by the inverse exponential relationship described above, may indicate thermal proximity to partial melt. Wysession *et al.* [2001] recently imaged a small-scale (~ 500 km diameter) low velocity anomaly at the CMB beneath Central America using ScS - S travel-time residuals. This purely elastic analysis could not distinguish between a compositional and thermal source for the observed anomalies. In our study, we isolate ScS - S differential attenuation in combination with differential travel-time anomalies to characterize the anomaly beneath Central America (Figure 1) as a likely thermal anomaly.

2. Method

[5] We assume differential attenuation and travel-time anomalies accumulate near the ScS bounce point where the two ray paths diverge most. The differential travel-time residual is expressed as $\delta T = [T_{ScS}-T_S]_{\text{Obs}} - [T_{ScS}-T_S]_{\text{PREM}}$, where T_{ScS} and T_S are the observed and PREM travel times for each ray path. We measure the observed travel-time residuals with the cross-correlation method following Wysession *et al.* [2001]. Each ray path is traced through an PREM model [Dziewonski and Gilbert, 1976] to produce the theoretical travel times.

[6] Differential attenuation is expressed in a similar manner, $\delta t^* = t_{ScS}^* - t_S^*$, where t_{ScS}^* and t_S^* are the observed attenuation values for the ScS and S phases, respectively. We measure differential attenuation in the frequency

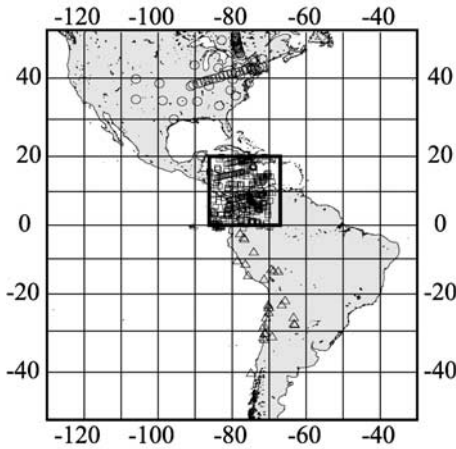


Figure 1. A map of the study region (large square), events (triangles), and stations (circles) used. The shaded squares at the center represent to bounce points of the ScS ray path.

domain using two techniques. We assume the S phase matches the ScS phase after convolution with a smoothed filter, $T(t)$. We estimate this filter, or transfer function, through ScS/S spectral division. Prior to spectral division we apply a moving-average filter to each phase to reduce the effects of narrow band spectral gaps. Each phase is windowed, tapered, and padded following *Wysession et al.* [2001] to retain maximum spectral information. The first method measures differential attenuation as the slope of the linearized ScS/S transfer function in the frequency domain between 10 and 150 mHz [*Bhattacharyya and Masters, 1996*]: $\delta t^* = \frac{\Delta(\log[T(\omega)])}{\Delta\omega}$. The slope of the linearized amplitude spectrum of each phase represents the attenuation of that phase for the same frequency range. The second method measures differential attenuation as the difference between the attenuation values of the two phases [e.g., *Flanagan and Wiens, 1994*]: $\delta t^* = \frac{\Delta(\log[ScS(\omega)])}{\Delta\omega} - \frac{\Delta(\log[S(\omega)])}{\Delta\omega}$. When the two techniques return identical results for δt^* , the amplitude spectrum is well represented for all frequencies of both phases. Otherwise, spectral gaps render the data unreliable. We attenuate the S phase by the attenuation operator, δt^* , to determine an improved ScS - S travel-time residual using the cross-correlation method. This residual is also corrected by δt^* to remove the dispersive effects of attenuation.

[7] For each reliable record we trace S and ScS ray paths through the ellipticity-corrected PREM radial quality factor model, which provides theoretical differential attenuation operators, $\delta t_{PREM}^* = \int_0^{T_{ScS}} 1/Q_{PREM} dt - \int_0^{T_S} 1/Q_{PREM} dt$. By changing the D'' quality factor, $Q_{\mu}(D'')$, from 4% to 400% of the PREM value at an interval of 4%, we obtain a wide range of theoretical differential attenuation operators. We also change the thickness of D'' from 50 km to 350 km at intervals of 50 km. The values of theoretical δt^* vary with distance. The most representative $Q_{\mu}(D'')$ and D'' thickness pair for a particular lateral sub-region is such that the least-squares error between theoretical and observed δt^* for all epicentral distances is minimized. For the purpose of simplicity we choose a single D'' thickness for the entire region and allow only $Q_{\mu}(D'')$ to change. We determine velocity in the exact same manner as quality factor, but with $V_{\beta}(D'')$

bounds running from 70% to 130% of PREM at an interval of 1%, where $dT = \int_0^{T_{ScS}} x/V_{PREM} dt - \int_0^{T_S} x/V_{PREM} dt$.

[8] We select only seismic records with high signal-to-noise ratios, where both the S and ScS phases may be clearly isolated. Event criteria include earthquakes with $M_b \geq 5.8$, recorded at epicentral distances between 40 and 80 degrees, where the ScS bounce points lay within the study region. The epicentral distance restriction reduces the chance of contamination due to SS and SKS interference. Records with low normalized ScS - S correlation are omitted. Broadband data from both temporary and permanent seismic arrays (GSN) increase the detail and breadth of the study area. The tighter station spacing of temporary seismic arrays, such as Missouri-to-Massachusetts (MOMA) and Lithoprobe Abitibi-Grenville geologic transect (ABITIBI), allows for better sampling in a small area from a single earthquake. This experiment uses 292 tangential component ScS and S records that fit the described criteria between 1993 and 1998 (Figure 1).

[9] We ensure the robustness of the data by normalizing and stacking S and ScS phases with similar paths in both the time and frequency domain. The normalization prior to stacking equalizes the weighting of each spectrum and therefore each attenuation operator. We stack in both the frequency and time domain to ensure that the resultant stacked signal is independent of the stacking method.

3. Results

[10] Comparison between data and stacks from similar earthquake-to-station ray paths indicates that the described criteria are sufficient to remove waveforms with spectral gaps. The relative amplitudes of individual waveforms that make up a stack often deviate from each other, but the shape of the distribution often remains constant. This is expected for sources with differing magnitudes and focal mechanisms. After normalization, the least-squares error between stacked attenuation operators and their constituent attenuation operators were less than 0.5 seconds for each of three distinct regions. While high, this error is only 10–20% of the observed anomalies. We find the same margin of error for the attenuation corrected travel-time residuals. In Figure 2 we provide an example of a single waveform to demonstrate the high quality of the data.

[11] Our un-attenuated travel-time residuals (Figure 3A) are similar to those observed by *Wysession et al.* [2001]. The differential attenuation (Figure 3B) and attenuation corrected travel-time residuals (Figure 3C) positively correlate with un-attenuated travel-time residuals. Adjusting travel-time calculations with attenuation alters the travel-time distribution from a positively skewed distribution with a mean δT of 0.25 s and maximum peak of -0.5 ± 0.25 s to a symmetric distribution with mean and peak at -0.75 ± 0.25 s.

[12] As a result of including attenuation in this study, the lateral scale of the positive travel-time anomaly decreases by $\sim 50\%$ to a diameter of ~ 250 km (Figure 3A versus Figure 3C). A larger high-velocity low-attenuation region surrounds the low-velocity high-attenuation region. This highly attenuating region (point X) has mean differential attenuation and travel-time anomalies of 2.6 seconds each. The low attenuating region (point Z) has mean differential attenuation and travel-time anomalies of -0.7 and -2.3 seconds respectively. Both measurements for the mid point

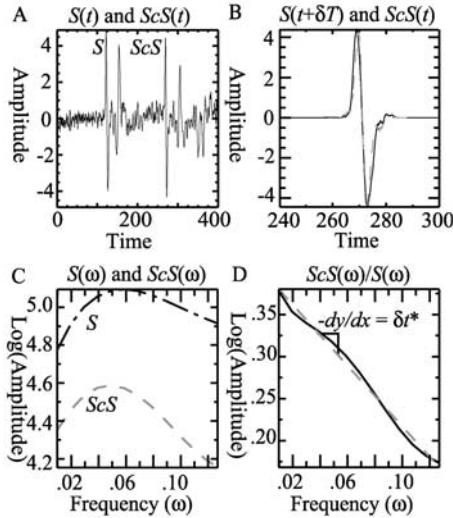


Figure 2. An example of the high-quality data used in this study is shown here as (A) the windowed S and ScS phases, (B) the S phase aligned with the ScS phases, (C) the smoothed S and ScS amplitude spectra, and (D) the differential attenuation, δt^* , as the linearized slope of the ScS/S transfer function amplitude spectrum.

(point Y) are indistinguishable from 0 seconds. While these values change marginally depending on the locations chosen, the structure remains essentially constant. Note that Figures 3A and 3C use PREM as reference models, so differences between the two are independent of the reference model. The resolution discussed here is at the level of the Fresnel zones for the ray paths, so the exact shape of the anomaly cannot be determined with this data set. The differential attenuation anomalies and differential travel-

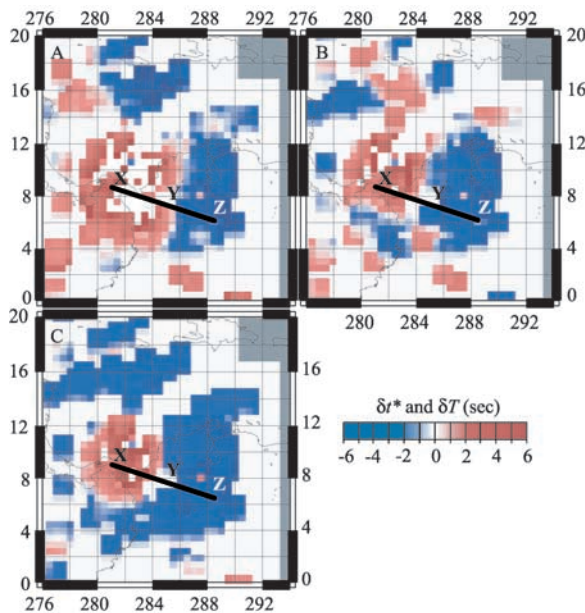


Figure 3. The seismic anomaly is shown here as (A) purely elastic travel time anomaly, (B) purely attenuation, and (C) elastic travel time anomaly corrected for attenuation. Grey sections had insufficient data. The same PREM reference model was used for normalizing both A and C.

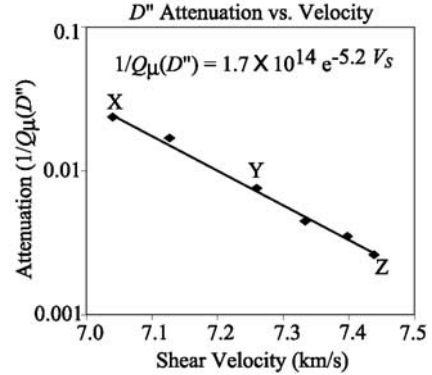


Figure 4. This figure shows the computed $Q_{\mu}(D'')$ vs. shear velocity as calculated for a 200 km thick layer at the CMB, using PREM values for all non D'' layers. The $Q_{\mu}(D'')$ and velocity values are calculated from the six observed δt^* and δT values at and between points X, Y, and Z shown in Figure 3. The equation demonstrates the exponential least-squares relationship between $Q_{\mu}(D'')$ and shear velocity. While the constants change due to starting with different models, the exponential nature does not.

time residuals are more strongly correlated with the ScS ($R^2 = 0.45$) anomalies than the S anomalies ($R^2 = 0.10$).

4. Discussion and Conclusions

[13] As with *Wysession et al.* [2001], we conclude that similarities between S and ScS paths sufficiently remove anomalies due to upper mantle anomalies such as the subducted Farallon slab. At the present time we have no ability to correct differential attenuation for epicentral distance. While the raw data may not account for epicentral distance, the calculated velocity and quality factor for each data point do. For this reason we analyze the relationship between D'' quality factor and velocity rather than differential attenuation and travel time. The bias introduced by selecting a D'' thickness affects quality factor and velocity proportionally for each data point. We reduce the bias by solving for quality factor and velocity using multiple D'' thickness.

[14] Forward modeling indicates that a thick ($\sim 200 \pm 50$ km) thermal anomaly could easily explain the observed attenuation and travel-time anomaly. Theoretical calculations show that δt^* variations on the order of the observed values are attainable by varying the D'' quality factor, $Q_{\mu}(D'')$. *Romanowicz* [1995] observes an inverse exponential relationship between quality factor and shear velocity, which is associated with a thermal anomaly in the upper mantle. We observe a similar relationship (Figure 4), and infer a thermal anomaly in the lower mantle. Values for $Q_{\mu}(D'')$ vary depending on the starting model, but still maintain an exponential relationship between velocity and attenuation. Models with mean $Q_{\mu}(D'')$ values comparable to those found in the upper mantle (≈ 110) require less extreme values of Q_{μ} for the low-attenuation regions than PREM [*Dziewonski and Anderson, 1981*]. Assuming that all anomalies are due to thermal variations within a 200 km thick isochemical D'' with mean $Q_{\mu}(D'')$ of 110, the high-attenuation anomaly has a Q_{μ} of ~ 70 , which is equivalent to the asthenosphere, and the low-attenuation region has Q_{μ} of ~ 350 , which is equivalent to PREM for the lower mantle.

Choosing the radial PREM $Q_{\mu}(D'')$ values as the mean value for any reasonable D'' thickness requires extremely high anomalous Q_{μ} values (in excess of 1200) to account for the low-attenuation region and produces non-representative differential attenuation values for the high attenuation region.

[15] The estimated value for quality factor trades off with the thickness of the anomaly. This does not reduce the effectiveness of our method because differential attenuation detects the strength of a thermal anomaly, if not the size. Some thickness constraints may be inferred by the stability of theoretical results given the observed attenuation. An ultra-thin (<50 km) low-velocity high-attenuation layer requires extreme deviations in quality factor ($Q_{\mu}(D'') < 3\% Q_{\mu}(D'')_{\text{PREM}}$) and large variations in velocity ($\delta V_{\beta} > 15\%$) to account for the observations. Models with thicker anomaly thickness (~ 200 km) require more modest velocity and attenuation anomalies. Nonetheless, the anomaly could take the form of a narrow ULVZ at the CMB in the manner of *Garnero et al.* [1998]. The apparent lack of lateral elongation along the predominant ray path direction (north-south) suggests that either the anomaly is confined to the CMB or is actually elongated east-west. We choose a ~ 200 km thick anomaly to strike a balance between these two observations. While the exponential relationship between anelastic and elastic properties does not preclude other attenuating mechanisms, it lends credence to a thermal anomaly model.

[16] At least one mechanism must be responsible for creating lateral variations in thermal structure. It is unlikely that the convection patterns of the outer core could cause a significant thermal anomaly in D'' [*Bloxham and Gubbins*, 1987]. Therefore, the mechanism must be mantle derived. Subducted oceanic lithosphere may sink and pond as a second order effect of lower mantle convection/advection [*Rigden et al.*, 1988]. Core-mantle Fe-exchange may change the thermal conductivity and homologous temperature of material at the CMB [*Knittle and Jeanloz*, 1991]. Ancient subducted slabs may isolate lower mantle material from the convection cell [*Tan et al.*, 2001]. The latter hypothesis may explain why 1) colder (high Q_{μ} , high V_{β}) material surrounds a warm anomaly (low Q_{μ} , low V_{β}), 2) the thermal anomaly does not buoyantly rise into the mid and upper mantle, and 3) the anomaly is located near a historically active subduction zone. Such a thermal anomaly would cause thermal expansion, which could cause the volume to rise as a mantle plume if the volume reached the critical Rayleigh number.

[17] **Acknowledgments.** Thanks to Kristin Portle and the late Stephen Zatman for their invaluable time and discussion. We thank IRIS PASSCAL for facilitating temporary broadband seismic deployments such as MOMA and ABITIBI, and the IRIS DMC for gathering and supplying the data used here. This material is based on work supported by the National Science Foundation under grants NSF-EAR-9629018 and NSF-EAR-0207751.

References

- Bhattacharyya, J., and G. Masters, Global lateral variation of shear wave attenuation in the upper mantle, *J. Geophys. Res.*, *101*, 22,273–22,287, 1996.
- Bloxham, J., and D. Gubbins, Thermal core-mantle interactions, *Nature*, *325*, 511–513, 1987.
- Dziewonski, A. M., and D. L. Anderson, Preliminary reference Earth model, *Phys. Earth Planet. Int.*, *25*, 297–356, 1981.
- Dziewonski, A. M., and F. Gilbert, The effect of small, aspherical perturbations on travel times and a re-examination of the corrections for ellipticity, *Geophys. J. R. Astron. Soc.*, *44*, 7–17, 1976.
- Flanagan, M. P., and D. A. Wiens, Radial upper mantle attenuation structure of inactive back arc basin differential shear wave measurements., *J. Geophys. Res.*, *99*, 15,469–15,485, 1994.
- Garnero, E. J., Heterogeneity of the lowermost mantle, *Annu. Rev. Earth Planet. Sci.*, *28*, 509–537, 2000.
- Garnero, E., J. Revenaugh, Q. Williams, T. Lay, and L. Kellogg, Ultra-low velocity zone at the core-mantle boundary, in *Constraints on the Core-Mantle Boundary Regionk Geodyn Ser.*, vol. 28, edited by M. Gurnis et al., pp. 319–334, AGU, Washington, D.C., 1998.
- Karato, S., Importance of anelasticity in the interpretation of seismic tomography, *Geophys. Res. Lett.*, *20*, 1623–1626, 1993.
- Karato, S., and H. A. Spetzler, Defect microdynamics in minerals and solid-state mechanisms of seismic wave attenuation and velocity dispersion in the mantle, *Rev. Geophys.*, *28*, 399–421, 1990.
- Knittle, E., and R. Jeanloz, Earth's core-mantle boundary: results of experiments at high pressure and temperature, *Science*, *251*, 1438–1443, 1991.
- Kuo, B.-Y., D. W. Forcyth, and M. E. Wysession, Lateral heterogeneity and azimuthal anisotropy in the North Atlantic determined from SS-S differential travel times, *J. Geophys. Res.*, *92*, 6421–6436, 1987.
- Rigden, S. M., T. J. Ahrens, and E. M. Stolper, Shock compression of molten silicates; results for a model basaltic composition, *J. Geophys. Res.*, *93*, 367–382, 1988.
- Romanowicz, B., A global tomographic model of shear attenuation in the upper mantle, *J. Geophys. Res.*, *100*, 12,375–12,394, 1995.
- Tan, E., M. Gurnis, and L. Han, Slabs in the lower mantle and their modulation of plume formation, *Geochem. Geophys. Geosyst.*, 2001.
- Wysession, M. E., K. M. Fischer, G. I. Al-eqabi, P. J. Shore, and I. Gurari, Using MOMA broadband array *ScS-S* data to image smaller-scale structures at the base of the mantle, *Geophys. Res. Lett.*, *28*, 867–870, 2001.

J. L. Fisher and M. E. Wysession, Department of Earth and Planetary Science, Box 1169, One Brookings Dr., St. Louis, MO 63130, USA. (jfisher@levee.wustl.edu)

K. M. Fischer, Department of Geological Sciences, Brown University, Providence, Rhode Island, USA.